Vol 8 No 1 (2026) E-ISSN: 2682-860X

International Journal on Robotics, Automation and Sciences

Impact of Image Pre-Processing and Optimizers on U-Net Segmentation of Prostate Cancer in MRI

Anis Amira Abdul Aziz, Haniza Yazid*, Nazahah Mustafa, Saufiah Abdul Rahim and Mohd Hanafi Mat Som

***Abstract* – Prostate cancer remains among the most frequently diagnosed cancers in men and is a significant issue in achieving timely and accurate diagnosis. Magnetic Resonance Imaging (MRI) is widely used because it can capture high-resolution anatomical information; however, cancer regions must be manually segmented, which is time-consuming and prone to variability among experts. This study proposes an automated segmentation algorithm utilizing the U-Net deep learning model, combined with image pre-processing techniques, to address these deficiencies. Median filtering was applied to remove salt-and-pepper noise, followed by brightness enhancement to enhance the intensity contrast of the images. The pre-processed images were used to train a U-Net model for segmenting prostate cancer. The Dice Similarity Coefficient (DSC) metric was used to evaluate segmentation accuracy. Three optimizers, Adam, RMSprop, and Adagrad, were tested. All of them were trained between 10 and 100 epochs. The Adam optimizer achieved the highest segmentation performance at epoch 90, with a DSC value of 0.9907, while RMSprop and Adagrad yielded 0.9888 and 0.9655, respectively. Pre-processing raised the mean DSC from 0.8206 to 0.8733, confirming its impact on image quality enhancement. Overall, the proposed method demonstrates high accuracy and reliability, offering a practical solution to support radiologists in prostate cancer diagnosis and treatment planning.**

Keywords—Prostate cancer, Magnetic Resonance Imaging (MRI), Image Segmentation, U-Net, Pre-processing, Dice Similarity Coefficient (DSC), Optimizer.

I. INTRODUCTION

Prostate cancer is one of the most prevalent cancers to affect men in the world, particularly men above the age of 50 [1]. The prostate is a walnut-sized organ below the bladder and in front of the rectum. The prostate plays an important role in the male reproductive system by secreting seminal fluid to nourish sperm and transport them. With growing age in men, the prostate may alter size and functionality, and abnormal cell growth can lead to cancer development [2]. According to global health statistics, prostate cancer is the second most common cancer

*Corresponding Author email: hanizayazid@unimap.edu.my, ORCID: 0000-0003-1760-2473
Anis Amira Abdul Aziz is with Faculty of Electronic Engineering & Technology, Universiti Malaysia Perlis, Campus Pauh Putra, 02600 Arau Perlis, Malaysia. (email: anisamira403@gmail.com)
Haniza Yazid is with Faculty of Electronic Engineering & Technology, Universiti Malaysia Perlis, Campus Pauh Putra, 02600 Arau Perlis, Malaysia. (email: hanizayazid@unimap.edu.my)
Nazahah Mustafa is with Faculty of Electronic Engineering & Technology, Universiti Malaysia Perlis, Campus Pauh Putra, 02600 Arau Perlis, Malaysia. (email: nazahah@unimap.edu.my)
Saufiah Abdul Rahim is with Faculty of Electronic Engineering & Technology, Universiti Malaysia Perlis, Campus Pauh Putra, 02600 Arau Perlis, Malaysia. (email: saufiah@unimap.edu.my)
Mohd Hanafi Mat Som is with Faculty of Electronic Engineering & Technology, Universiti Malaysia Perlis, Campus Pauh Putra, 02600 Arau Perlis, Malaysia. (email: mhanafi@unimap.edu.my)

International Journal on Robotics, Automation and Sciences (2026) 8, 1:104-112
https://doi.org/10.33093/ijoras.2026.8.1.11
Manuscript received: 9 Oct 2025 | Revised: 5 Dec 2025 | Accepted: 26 Feb 2026 |
Published: : 31 Mar 2026

Published by MMU PRESS. URL: http://journals.mmupress.com/ijoras

diagnosed in men and remains one of the top causes of cancer-related death. Early detection is crucial for maximizing treatment outcomes and improving survival rates. Prostate-specific antigen (PSA) blood test, digital rectal examination (DRE), and other more advanced imaging studies, such as MRI, are routine screening methods for prostate cancer. Among these, MRI is highly effective as it can produce high-contrast, high-resolution images of soft tissues; hence, it is highly appropriate for identifying abnormalities in the prostate [3].

Even with benefits, prostate MRI image interpretation remains challenging. The internal anatomy of the prostate comprises several zones, namely the Peripheral Zone (PZ), Transitional Zone (TZ), and Central Zone (CZ). Each zone has unique tissue properties. Most prostate cancers occur in the peripheral zone [4]. However, the boundaries of the zones may not be clearly defined, especially in low-quality imaging. Thus, radiologists manually segment prostate regions that are often labor-intensive, time-consuming, and subject to variability depending on the expertise of the observer. To overcome these limitations, the use of automated segmentation techniques based on deep learning has gained considerable interest. Convolutional Neural Networks (CNNs), particularly the U-Net architecture, have demonstrated remarkable performance in biomedical image segmentation tasks due to their encoder–decoder design and ability to learn spatial features effectively.

This paper focuses on implementing a U-Net-based segmentation framework designed to identify and delineate prostate cancer regions in MRI images. The method incorporates pre-processing steps such as median filtering and brightness enhancement to improve image clarity before training the segmentation model. This approach aims to reduce reliance on manual annotation, improve segmentation accuracy, and support faster and more consistent diagnosis of prostate cancer.

II. REVIEW OF PROSTATE CANCER SEGMENTATION

Prostate cancer segmentation on MRI images is important for correct diagnosis, treatment planning, and follow-up. Several computational procedures have been suggested over the years to improve the reliability and efficiency of prostate cancer segmentation. The procedures can be broadly classified under four categories: traditional approaches, machine learning, deep learning, and hybrid methods.

A. Conventional Techniques

Early segmentation techniques in medical imaging primarily employed conventional image processing algorithms such as thresholding, region growing, and edge detection. These algorithms use pixel intensity and basic geometric features to detect anatomical structures. Although computationally simple and fast, they work poorly for low-contrast images or intricate anatomical shapes. For example, Gong et al. [5] applied region-growing algorithms based on radiomic features but reported that they were MRI quality- and non-uniformity-sensitive across patients. Shanmugalingam et al. [6] employed multi-level Otsu thresholding, which successfully detected intensity transitions but was unable to capture fine anatomical details and was sensitive to noise. Similarly, the atlas-based segmentation explored by Chen et al. [7] performed well for average prostate shapes but struggled significantly with anatomical distortions.

Machine learning (ML) offered prostate cancer segmentation new hope by exploiting data-driven classification. Algorithms such as k-nearest neighbours (k-NN), support vector machines (SVM), and random forest models have been encouraging. However, these models were driven by manually crafted features, such as shape, texture, and intensity, which may lack a generalized ability across datasets. For instance, Anand et al. [8] utilized GLCM texture features in conjunction with k-NN, achieving 91.67% accuracy; however, the method proved to be extremely noise-sensitive and performed poorly when the datasets were large. Wang et al. [9] used a random forest classifier on radiomic features and achieved 88.2% sensitivity and 89.6% specificity. Li et al. [10] employed an SVM-based method utilizing radiomic intensity features, achieving 90.1% accuracy; however, its performance declined drastically in low-contrast conditions.

B. Conventional Techniques

Recent years have seen a significant improvement in the task of medical image segmentation using deep learning, particularly with Convolutional Neural Networks (CNNs). In contrast to traditional ML methods, deep learning networks have automatically learned relevant features from data, restricting the need for manual feature engineering. The U-Net model, renowned for its encoder–decoder structure with skip connections, has become the most well-liked model for biomedical image segmentation. Several studies have shown the success of U-Net in segmenting prostate cancer regions from MRI scans. Aldoj et al. [11] proposed Zone-U-Net and CSPCa-U-Net, achieving Dice scores of 0.78 (PZ), 0.86 (CG), and 0.89 (whole prostate), respectively, highlighting the benefits of zone-by-zone training. Pellicer-Valero et al. [12] proposed Retina U-Net, a combined detection and segmentation model that yielded an AUC of 0.96 with 1.00 sensitivity and 0.79 specificity. Rui Jin et al. [13] evaluated the baseline U-Net model on the PROSTATEx dataset, obtaining Dice scores ranging from 0.80 to 0.95, which confirmed U-Net's capability in handling challenging prostate anatomy and variability.

In order to even further enhance segmentation performance, hybrid models have been proposed, combining different techniques such as deep learning, optimisation algorithms, and traditional image processing. These tend to increase the level of accuracy and boundary sharpening but require more computationally intensive processes. For example, Paulo Lapa et al. [14] introduced CRF-XmasNet, a model that combines Conditional Random Fields (CRFs) and CNNs, improving spatial coherence and reducing boundary errors. Nevertheless, the intricate nature of the model created challenges during integration. Reddy et al. [15] introduced the LHFGSO-DMN model, which combined deep learning and heuristic optimization, achieving higher accuracy (94.63%), sensitivity (93.46%), and specificity (95.72%). However, feature stability was a problem. Saqib Iqbal et al. [16] studied a hybrid ensemble involving ResNet-101, LSTM, SVM, k-NN, and Naïve Bayes. Of the above, the model with k-NN–Cosine similarity had an accuracy of 98.95% and an AUC of 0.966. However, the complexity and computational cost of the ensemble were difficult for real-time clinical applications.

A critical evaluation of existing segmentation methods reveals that while manual and machine learning-based methods have been significant contributors to the field, they are lacking in solving intricate anatomical variations, poor image contrast, and noise in prostate MRI scans. Deep learning methods, particularly those based on U-Net, have performed relatively better as they can learn hierarchical features and capture contextual information. However, the quality of such models is still influenced by image quality and pre-processing operations. This study proposes an enhanced segmentation framework utilizing a U-Net model, supported by pre-processing techniques such as median filtering and brightness adjustment, to improve the clarity and contrast of prostate MRI images. The technique aims to reduce segmentation error, enhance model generalizability, and improve overall accuracy in prostate cancer area detection.

III. PROPOSED METHODOLOGY

This study presents a prostate cancer segmentation framework using a deep learning approach based on the U-Net architecture. The overall process consists of four main phases, as presented in the flowchart in Figure 1. All MRI slices were loaded as single-channel grayscale images and converted to tensors from the torchvision library, which scales pixel intensities to the {0,1} range. The images were used at their original resolution, and no data augmentation techniques were applied (rotation, flipping, scaling). In this work, all experiments were conducted directly on the pre-processed images after median filtering and brightness enhancement.

A. Dataset

This study obtained the dataset from an open-source repository hosted on GitHub, specifically the PROSTATEx dataset [17]. The dataset comprises 687 prostate Magnetic Resonance Imaging (MRI) scans, each accompanied by a corresponding segmentation mask. It includes T2-weighted MRI sequences that provide high-resolution anatomical details of the prostate structure. In addition, the dataset includes Diffusion-Weighted Imaging (DWI), which provides functional imaging data that enhances the differentiation between cancerous and non-cancerous prostate tissues. The MRI data were acquired in three standard anatomical planes, which are axial, sagittal, and coronal. These planes are used to represent the spatial structure and orientation of the prostate gland. Although the PROSTATEx dataset includes T2 and DWI sequences, this study uses only T2-weighted axial slices, as it offers the most detailed visualization of prostate zones and provides clearer indications of cancerous regions. The segmentation masks provided in the dataset, which experienced radiologists annotated, serve as the ground truth and are used for training, validation, and evaluation of the deep learning segmentation model. The dataset was divided into 70% training, 15% validation, and 15% testing. Slices from the same patient were kept within the same partition to prevent data leakage. In this work, model selection and hyperparameter tuning were performed exclusively using the validation set.

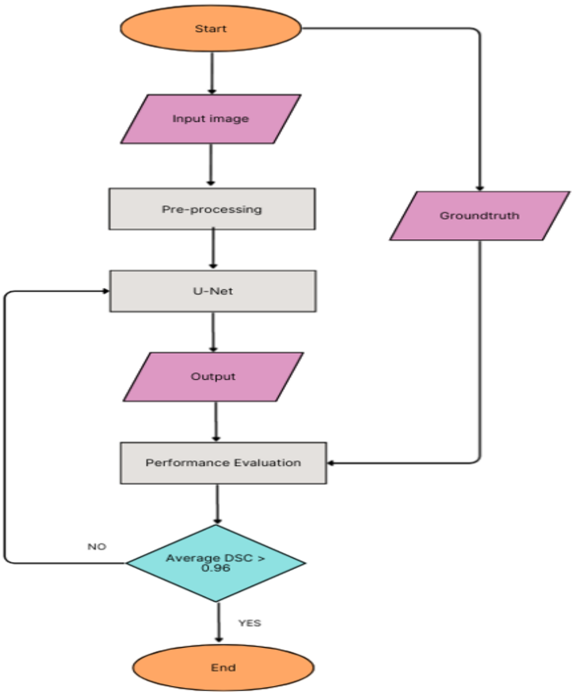

FIGURE 1. Flowchart of the MRI Segmentation for Prostate Cancer.

B. Image Pre-processing

The prostate MRI images obtained from the PROSTATEx dataset may have several imperfections that negatively impact the performance of the segmentation task. These imperfections are typically caused by factors such as the patient's motion during scanning, imaging parameters, magnetic field inhomogeneities, and inherent anatomical variations. As a result, the images may exhibit noise, low contrast, and blurred tissue boundaries. To address these issues, a pre-processing phase was employed to enhance the overall image quality of the input images prior to training the deep learning model. The primary objective of this phase is to enhance visual clarity, highlight major anatomical structures, and reduce image noise, thereby enabling more accurate segmentation. This study employed a pixel-based pre-processing method, where the intensity values of every pixel in the image were adjusted to better represent the features. Pre-processing involves two major operations: median filtering and illumination enhancement. These two operations are performed consecutively to ensure MRI images fed into the model for segmentation are optimized in terms of clarity and uniformity.

C. Median filtering

Median filtering is applied as the initial step in the pre-processing pipeline to remove salt-and-pepper noise, a common artifact in MRI images. The noise, often caused by magnetic interference or acquisition artifacts, can obscure fine structural details and impact segmentation performance if left unaddressed. The median filter replaces each pixel value with the median of its surrounding neighborhood [18]. This method excels at removing isolated points of noise and preserving edges, making it suitable for medical images where anatomical boundary integrity must be preserved [19]. Median filtering, when applied, contributes to global visualization of the prostate region by deleting noise without creating significant blurring. The resulting image in Figure 2 is a cleaner image with less noise, and the deep model can achieve segmentation more effectively.

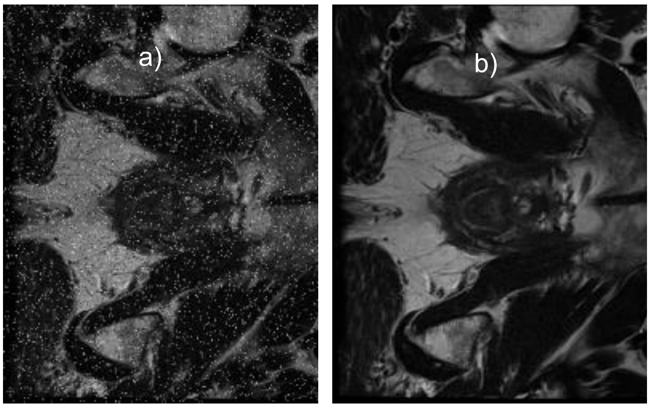

FIGURE 2. Pre-processing phase a) Original MRI image b) Median filtered image.

D. Brightness Enhancement

Brightness enhancement is performed after the noise reduction process to improve the overall visibility of prostate structures in the MRI images. Original MRI scans often suffer from low contrast, which can make it difficult to distinguish between healthy tissue and regions affected by cancer. Enhancing the brightness helps highlight important anatomical features, especially the boundaries between prostate zones [20]. This process adjusts the intensity values of the image to improve the difference between foreground and background areas. As a result, regions of interest become more visible, which supports better learning during the training phase of the segmentation model. Brightness enhancement also reduces the risk of under-segmentation or over-segmentation caused by low contrast input images. Brightness enhancement was implemented per-slice as a linear intensity scaling operation, where every pixel value was multiplied by a fixed factor (default = 2.0) and clipped to the valid 0–255 range. This simple global enhancement increased overall visibility and improved contrast of prostate boundaries without introducing non-linear distortions. As presented in Figure 3, brightness enhancement is applied after median filtering to improve the overall clarity of the MRI image.

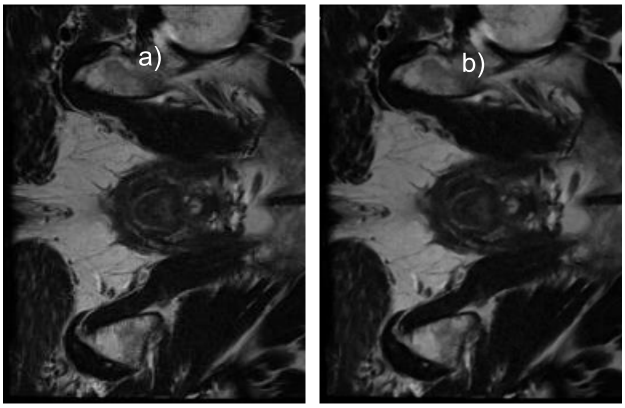

FIGURE 3. Pre-processing phase a) Median filtered image b) Brightness enhanced image.

E. U-Net Architecture

The U-Net architecture is used in this study due to its strong performance in biomedical image segmentation. It is well known for its ability to work with small datasets and for preserving spatial information, which is important in segmenting complex anatomical structures such as the prostate. The architecture of the U-Net model is shown in Figure 4. Model training was performed on a workstation equipped with an Intel® Core™ i7-6700HQ CPU (2.60 GHz), 16 GB RAM, and an NVIDIA GeForce GTX 950M GPU (4 GB VRAM), running a 64-bit operating system with CUDA-enabled PyTorch.

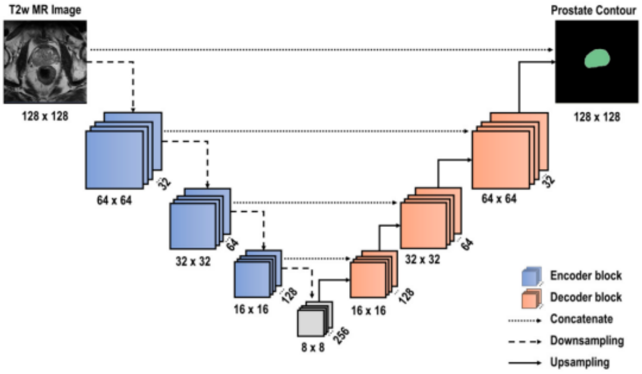

FIGURE 4. U-Net architecture for prostate cancer segmentation

The U-Net architecture consists of two main stages: the downsampling path and the upsampling path. The downsampling path is responsible for extracting features and reducing the image size using convolutional layers followed by max pooling. This helps the model understand the input image's overall context by capturing deeper features at each level. After the downsampling process, the upsampling path aims to recover the original image resolution. It utilizes upsampling layers to increase the spatial dimensions gradually and combines the upsampled features with those from the corresponding downsampling layers. This combination is achieved through skip connections, which enable the model to retain important spatial details that are often lost during downsampling. After undergoing several layers of downsampling and upsampling, the network concludes with a final convolutional layer, followed by a sigmoid activation function, to produce a binary segmentation mask. This mask highlights the region of interest, which in this case is the cancerous area within the prostate [21].

The U-Net model was trained to segment prostate cancer regions from MRI images using different optimization strategies. Three optimizers were compared in this study, namely Adam, RMSprop, and Adagrad. Each optimizer has a distinct update rule, which was tested to assess its impact on segmentation performance. Binary Cross-Entropy with Logits Loss was selected as the loss function, which is suitable for binary classification tasks, such as distinguishing between cancerous and non-cancerous tissue in MRI scans. The input images and their corresponding ground truth masks were loaded using a custom dataset class during training. A batch size of 4 was used to accommodate GPU memory constraints, and the learning rates were fixed at 0.0001 for Adam and RMSprop, while Adagrad utilized a higher learning rate of 0.004 to enhance convergence. The training process was carried out for 110 epochs for each optimizer. The model parameters were updated at each epoch through backpropagation and optimizer-specific weight updates. The training loss was monitored throughout the training phase, and segmentation performance was evaluated based on the Dice Similarity Coefficient (DSC). The optimizer configurations used in this study are summarized in Table 1.

TABLE 1. A summary of the results with and without pre-processing.

Parameter	ADAM	RMSprop	AdaGrad
Learning Rate	0.0001	0.0001	0.004
Batch Size	4	4	4
Epochs	100	100	80
Loss Function	Binary Cross-Entropy with Logits	Binary Cross-Entropy with Logits	Binary Cross-Entropy with Logits
Evaluation Metrics	Dice Similarity Coefficient (DSC)	Dice Similarity Coefficient (DSC)	Dice Similarity Coefficient (DSC)

Performance evaluation is a crucial step in assessing the effectiveness of the proposed segmentation model [22]. It is done by comparing the predicted segmentation output with the ground truth annotation, using a suitable metric to measure how accurately the model identifies the regions of prostate cancer. In this study, the Dice Similarity Coefficient (DSC) is used as the main evaluation metric. DSC is a widely accepted statistical measure that calculates the overlap between two binary segmentation results. It is especially suitable for medical image segmentation, where the accuracy of region boundary detection is essential for diagnosis and treatment planning. The DSC is calculated by measuring the size of the intersection between the predicted segmentation and the ground truth, relative to the total size of both sets. The formula for DSC is given in Equation (1).

$$DSC = \frac{2 \times |A \cap B|}{|A| + |B|} \quad (1)$$

where:

A is the predicted segmentation output

B is the ground truth segmentation

$A \cap B$ is the intersection area between the two masks

The range of DSC is 0 to 1. A value of overlap of 1 indicates that the predicted mask and ground truth completely overlap with each other, while a value of overlap of 0 indicates that no overlap exists. In the segmentation of prostate cancer, a high DSC value indicates that the model can effectively identify and delineate cancerous regions, which is essential for decision-making in treatment. Using DSC as the measurement criterion allows the model to be measured quantitatively and objectively. It can also be used to compare performance across optimizers, pre-processing methods, and model configurations.

IV. Results And Discussion

This section presents the experimental results of the prostate cancer segmentation model, utilizing the U-Net architecture. The evaluation was conducted on two levels, involving a visual inspection of segmentation outcomes and a quantitative analysis using the Dice Similarity Coefficient (DSC). The outcomes are organized to highlight the impact of the image pre-processing, the trend in the model performance throughout epochs, and comparisons among different optimizers. All results are presented in terms of the model's ability to learn and generalize from prostate MRI images.

A. Effect of Pre-processing

Pre-processing is a crucial step in medical image segmentation, as it significantly influences the clarity of the input data. In this study, two pre-processing techniques were applied, namely median filtering and brightness enhancement. These were designed to reduce noise and enhance the contrast of the MRI images. The original prostate MRI images contained considerable noise and low intensity contrast, which could negatively affect model learning. Median filtering was applied to reduce the presence of noise while preserving the important structural boundaries. This type of noise often appears due to acquisition conditions and can cause the model to misclassify pixels. The second pre-processing step involved brightness enhancement, which increased the contrast between the prostate tissue and its surrounding structures. This step helped highlight the prostate boundaries more clearly, making it easier for the model to distinguish between cancerous and non-cancerous regions. The visual improvements are shown in Figure 5. The original image is difficult to interpret due to noise and poor contrast. After filtering and brightness adjustment, the prostate structure becomes more defined.

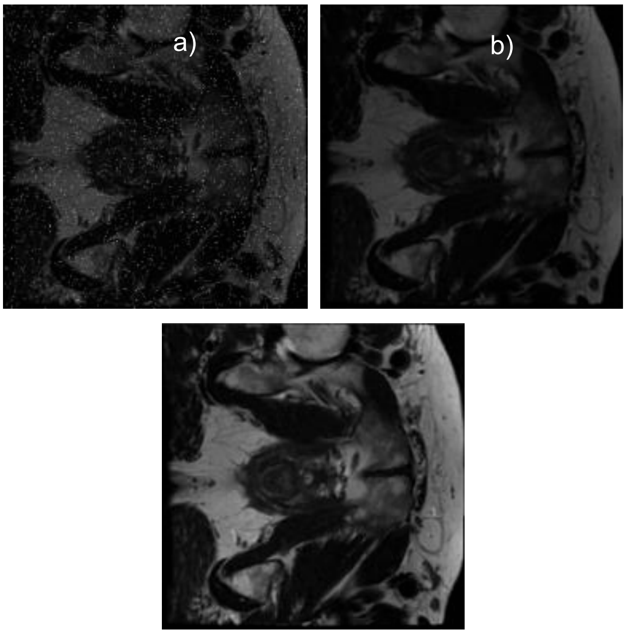

FIGURE 5. Pre-processing phase a) Original MRI image b) After median filtering c) After brightness enhancement.

A quantitative comparison was also conducted to evaluate the impact of pre-processing on model performance. When the model was trained without pre-processing, the segmentation results were inconsistent and produced a lower average DSC value. After applying the pre-processing steps, the model achieved a more stable segmentation performance. This is evident in Table 2.

TABLE 2. Comparison of average DSC with and without pre-processing.

Pre-processing	Average DSC
With Pre-procesing	0.8733
Without Pre-processing	0.8206

B. Optimizer Performance Based on Image-Level DSC

To compare the influence of each optimizer on model learning in more detail, the segmentation results were recorded at various training epochs on sample images. Segmentation output was visually compared and augmented with single DSC values. For the Adam optimizer, segmentation at epoch 10 was poor. The predicted mask was blurry, and the model was unable to differentiate the entire structure of the prostate. The model improved greatly at epoch 30. The prostate boundaries were more accurately segmented, although some small areas were still missed. The model performed best visually at epoch 90, with a well-defined contour of the prostate and few false regions. The image-level DSC was 0.9899 at epoch 90, indicating that the predicted mask was nearly identical to the truth as denoted in Figure 6. The results are presented in Figure 7.

FIGURE 6. Ground truth for the sample result

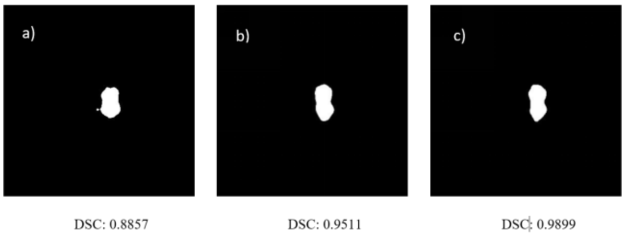

FIGURE 7. Adam optimizer output at different epochs a) Epoch 10 b) Epoch 30 c) Epoch 90.

At epoch 10, the segmentation was less accurate with a DSC of 0.7898, and the output appeared fragmented. The model improved at epoch 30 and reached its best performance at epoch 90 with a DSC of 0.9890. Compared to Adam, RMSprop took more epochs to achieve this level of accuracy. Figure 8 illustrates this progression.

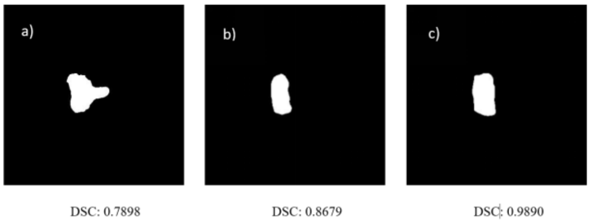

FIGURE 8. RMSprop optimizer output at different epochs a) Epoch 10 b) Epoch 30 c) Epoch 90.

Adagrad performed less consistently. In early epochs, the segmentation was poor, and the prostate shape was not clearly identified. Even though the model gradually improved, its best segmentation was achieved at epoch 70 with a DSC of 0.8659. Compared to Adam and RMSprop, Adagrad produced more false-positive and false-negative regions, and its learning rate appeared to plateau earlier. Figure 9 presents the progression of Adagrad's results.

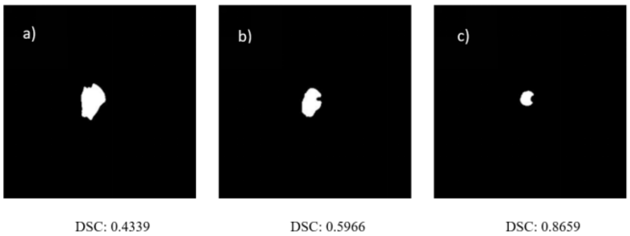

FIGURE 9. Adagrad optimizer output at different epochs a) Epoch 10 b) Epoch 30 c) Epoch 70.

These results confirm that the choice of optimizer plays a crucial role in segmentation performance. Adam was the most stable and accurate, followed by RMSprop, while Adagrad was more sensitive to parameter settings and had slower learning.

C.Average DSC by Epoch

In addition to visual inspection, the average DSC for each epoch was computed to evaluate the overall learning trend of each optimizer. This analysis helps determine the final accuracy, how quickly the model converges, and whether it exhibits any signs of overfitting or stagnation. Adam showed a steady improvement in average DSC from epoch 10 to epoch 90, reaching a peak of 0.9907. This indicates that the model continuously learned more accurate features over time. After epoch 90, a slight drop in performance was observed, marking the beginning of overfitting. RMSprop also improved over time, reaching a maximum average DSC of 0.9888 at epoch 90. Its learning curve was slightly slower than Adam's, but the final performance was still high and stable. The performance remained nearly constant after epoch 90. Adagrad showed faster early growth but plateaued earlier than the other two optimizers. The highest average DSC was 0.9655 at epoch 70. After that, no significant improvements were observed. This suggests that Adagrad may require further adjustments to its hyperparameters to perform at the same level as Adam or RMSprop. The comparison of average DSC values across optimizers is presented in Table 3.

TABLE 3. Summary of Average DSC for all Optimizers.

Epoch	ADAM	RMSprop	AdaGrad
Epoch 10	0.9142	0.8825	0.8732
Epoch 20	0.9534	0.9201	0.9180
Epoch 30	0.9664	0.9498	0.9384
Epoch 40	0.9749	0.9609	0.9444
Epoch 50	0.9801	0.9722	0.9507
Epoch 60	0.9836	0.9730	0.9529
Epoch 70	0.9858	0.9780	0.9655
Epoch 80	0.9876	0.9783	0.9578
Epoch 90	0.9907	0.9888	-
Epoch 100	0.9822	0.9887	-

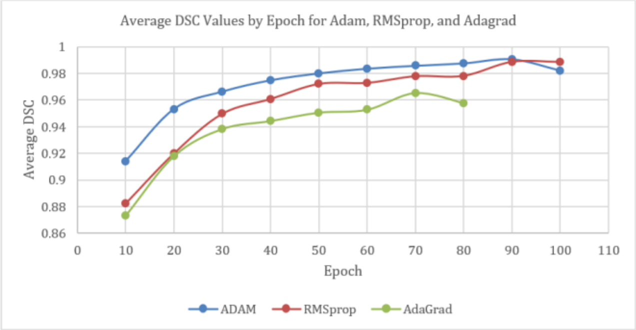

FIGURE 10. Average DSC Values by Epoch for Adam, RMSprop and Adagrad.

The results support the conclusion that Adam is the most effective optimizer for this task under the tested conditions. RMSprop is a good alternative, while Adagrad may require specific tuning to reach similar performance.

To provide a clearer view of the segmentation accuracy progress over training, a line graph was plotted to show the mean Dice Similarity Coefficient (DSC) values for all epochs for each optimizer. As shown in Figure 10, the Adam optimizer achieved the highest DSC throughout the entire training period, consistently improving from epoch 10 to epoch 90 before experiencing a slight drop. RMSprop showed similar growth, reaching its peak at epoch 90 as well. However, Adagrad showed slower improvement than the other optimizers, and its performance began stabilizing earlier, with the highest average DSC recorded at epoch 70. The graph also shows the stability and reproducibility of Adam and RMSprop, whereas Adagrad showed more fluctuation and a slower learning curve. This graph supports the results in Table 3 and maintains that Adam performs optimally under the implemented conditions. Adam provided the best performance because it uses both first-moment (mean) and second-moment (variance) estimates of gradients, enabling more stable and adaptive learning-rate adjustments across layers. RMSprop relies only on second-moment normalization, which makes it more sensitive to noisy gradient variations and results in slower convergence. Adagrad accumulates squared gradients, causing its effective learning rate to shrink early during training, which can limit further improvement. Adam's bias-corrected adaptive updates therefore yield more consistent convergence behavior and better generalization, explaining the higher DSC values observed in the experiments.

V. CONCLUSION

The proposed framework included median filtering and brightness enhancement as pre-processing steps, followed by U-Net segmentation trained using Adam, RMSprop, and Adagrad optimizers. The application of pre-processing techniques yielded clearer and more consistent MRI images, which significantly enhanced the model's learning ability. Quantitative analysis revealed that the average Dice Similarity Coefficient (DSC) increased from 0.8206 to 0.8733 with pre-processing, confirming the essential requirement of high-quality input images. The increase in mean DSC from 0.8206 to 0.8733 represents a consistent improvement across the evaluated test samples. Although the analysis remains descriptive due to dataset constraints, the observed trend indicates that median filtering and brightness enhancement contribute positively to segmentation accuracy. A more comprehensive statistical analysis will be considered in future work using larger datasets with standardized patient-level sample distributions. Among the three optimizers, Adam achieved the best segmentation performance. It recorded the highest image-level DSC of 0.9899 and the highest average DSC of 0.9907 at epoch 90. RMSprop performed equally well with a highest average DSC of 0.9888, while Adagrad was poorer, reaching its optimal DSC of 0.9655 at epoch 70. Overall, the results demonstrate that combining pre-processing and a U-Net-based model, supported by a suitable optimizer, can produce accurate and reliable segmentation of prostate cancer regions. Future work may include testing the model on larger and more diverse datasets, repeated training runs to further assess optimizer robustness, incorporating advanced architectures such as attention mechanisms, and exploring post-processing techniques to further refine the segmentation.

Acknowledgment

The authors would like to express their sincere appreciation to the anonymous peer reviewers for their valuable time, insightful comments, and constructive suggestions that greatly contributed to improving the quality and clarity of this manuscript.

Funding Statement

There is no funding agencies supporting the research work.

Author contributions

Anis Amira Abdul Aziz: Methodology, Analysis, Writing – Original Draft Preparation

Haniza Yazid: Conceptualization, Supervision, Methodology, Validation, Review & Editing

Nazahah Mustafa: Conceptualization, Validation, Review & Editing

Saufiah Abdul Rahim: Conceptualization, Methodology, Validation, Review & Editing

Mohd Hanafi Mat Som: Validation, Review & Editing

Conflict of interests

The authors declare no conflict of interest related to the publication of this manuscript

Ethics statements

Ethical approval was not applicable to this research since it did not involve human participants, animals, or sensitive data.

References

[1] M. Anzidei, A. Bazzocchi, C. Gagliardo, C. Catalano, A. Napoli and R. Scipione, "HIFU for Bone Metastases and other Musculoskeletal Applications," *Seminars in Interventional Radiology*, vol. 35, no. 04, pp. 261-267, 2018.
DOI: https://doi.org/10.1055/s-0038-1673363

[2] Z. Khan, N. Yahya, K. Alsaih, M.I. Al-Hiyali and F. Meriaudeau, "Recent Automatic Segmentation Algorithms of MRI Prostate Regions: A Review," *IEEE Access*, vol. 9, pp. 97878-97905, 2021.
DOI: https://doi.org/10.1109/ACCESS.2021.3090825

[3] B. Shaw, F.M. Walter, W. Hamilton and T. Martins, "Symptom appraisal and help seeking in males with symptoms of possible prostate cancer: a qualitative study with an ethnically diverse sample in London," *British Journal of General Practice*, vol. 73, no. 732, pp. e502-e510, 2023.
DOI: https://doi.org/10.3399/BJGP.2022.0554

[4] N.F. Wasserman, P. Murguan, B. Spilseth, G.J. Metzger and T. Sanghvi, "Peripheral Zone Enlargement: a newly described entity on MRI," *medRxiv*, 2020.
DOI: https://doi.org/10.1101/2020.04.03.20052290

[5] H. Gong, SLIC segmentation and texture feature extraction for a radiomic analysis of prostate cancer using multiparametric MRI *Master thesis, Eindhoven University of Technology,* 2024.

[6] K. Shanmugalingam, "Prostate Image Segmentation Using Deep Learning", *PhD Thesis, UNSW Sydney*, 2024.
DOI:https://doi.org/10.26190/unsworks/30491

[7] H. Chen, L. Kumaralingam, S. Zhang, S. Song, F. Zhang, H. Zhang, T. Pham, K. Punithakumar, E.H. Lou, Y. Zhang, L.H. Le and R. Zheng, "Neural implicit surface reconstruction of freehand 3D ultrasound volume with geometric constraints," *Medical Image Analysis*, vol. 98, pp. 103305, 2024.
DOI: https://doi.org/10.1016/J.MEDIA.2024.103305

[8] L. Anand, S. Mewada, W. Shamsi, M. Ritonga, N. Aflisia, P. KumarSarangi and M. NdoleArthur, "[Retracted] Diagnosis of Prostate Cancer Using GLCM Enabled KNN Technique by Analyzing MRI Images," *BioMed Research International*, vol. 2023, no. 1, 2023.
DOI: https://doi.org/10.1155/2023/3913351

[9] L. Wang, R. Sun, X. Wei, J. Chen, S. Jia, G. Wu and S. Nie, "Enhancing prostate cancer segmentation on multiparametric magnetic resonance imaging with background information and gland masks," *Medical Physics*, vol. 51, no. 11, pp. 8179-8191, 2024.
DOI: https://doi.org/10.1002/MP.17346

[10] X. Li, Z. Liu and L. Yang, "The artificial intelligence automatic diagnosis model based on the needle tissue of prostate ultrasound," *International Conference on Communication, Information, and Digital Technologies (CIDT2024)*, p. 23, 2024.
DOI: https://doi.org/10.1117/12.3033311

[11] P. Mehta, M. Antonelli, S. Singh, N. Grondecka, E.W. Johnston, H.U. Ahmed, M. Emberton, S. Punwani and S. Ourselin, "AutoProstate: Towards Automated Reporting of Prostate MRI for Prostate Cancer Assessment Using Deep Learning," *Cancers*, vol. 13, no. 23, pp. 6138, 2021.
DOI: https://doi.org/10.3390/CANCERS13236138

[12] O.J. Pellicer-Valero, J.L.M. Jiménez, V. Gonzalez-Perez, J.L.C. Ramón-Borja, I.M. García, M.B. Benito, P.P. Gómez, J. Rubio-Briones, M.J. Rupérez and J.D. Martín-Guerrero, "Deep learning for fully automatic detection, segmentation, and Gleason grade estimation of prostate cancer in multiparametric magnetic resonance images," *Scientific Reports*, vol. 12, no. 1, 2022.
DOI: https://doi.org/10.1038/S41598-022-06730-6

[13] R. Jin, D. Li, D. Xiang, L. Zhang, H. Zhou, F. Shi, W. Zhu, J. Cai, T. Peng and X. Chen, "AI-based Automatic Segmentation of Prostate on Multi-modality Images: A Review". 2024.
DOI:10.48550/arXiv.2407.06612

[14] P. Lapa, M. Castelli, I. Gonçalves, E. Sala and L. Rundo, "A Hybrid End-to-End Approach Integrating Conditional Random Fields into CNNs for Prostate Cancer Detection on MRI," *Applied Sciences*, vol. 10, no. 1, pp. 338, 2020.
DOI: https://doi.org/10.3390/APP10010338

[15] S.K. Reddy and K. Kathirvelu, "Hybrid Optimization Enabled Deep-Learning for Prostate Cancer Detection," *Sensing and Imaging*, vol. 25, no. 1, 2024.
DOI: https://doi.org/10.1007/S11220-024-00495-0

[16] S. Iqbal, G.F. Siddiqui, A. Rehman, L. Hussain, T. Saba, U. Tariq and A.A. Abbasi, "Prostate Cancer Detection Using Deep Learning and Traditional Techniques," *IEEE Access*, vol. 9, pp. 27085-27100, 2021.
DOI: https://doi.org/10.1109/ACCESS.2021.3057654

[17] R. Cuocolo, A. Stanzione, A. Castaldo, D.R.D. Lucia and M. Imbriaco, "Quality control and whole-gland, zonal and lesion annotations for the PROSTATEx challenge public dataset," *European Journal of Radiology*, vol. 138, pp. 109647, 2021.
DOI: https://doi.org/10.1016/j.ejrad.2021.109647

[18] H. Liang, N. Li and S. Zhao, "Salt and Pepper Noise Removal Method Based on a Detail-Aware Filter," *Symmetry*, vol. 13, no. 3, pp. 515, 2021.
DOI: https://doi.org/10.3390/SYM13030515

[19] J. Jian, L. Liu, Y. Zhang, K. Xu and J. Yang, "Optical Remote Sensing Ship Recognition and Classification

Based on Improved YOLOv5," *Remote Sensing*, vol. 15, no. 17, pp. 4319, 2023.
DOI: https://doi.org/10.3390/RS15174319

[20] L. Kong, M. Huang, L. Zhang and L.W.C. Chan, "Enhancing Diagnostic Images to Improve the Performance of the Segment Anything Model in Medical Image Segmentation," *Bioengineering*, vol. 11, no. 3, pp. 270, 2024.
DOI: https://doi.org/10.3390/BIOENGINEERING11030270

[21] M. Montazerolghaem, Y. Sun, G. Sasso and A. Haworth, "U-Net Architecture for Prostate Segmentation: The Impact of Loss Function on System Performance," *Bioengineering*, vol. 10, no. 4, pp. 412, 2023.
DOI: https://doi.org/10.3390/BIOENGINEERING10040412

[22] K.H. Zou, S.K. Warfield, A. Bharatha, C.M. Tempany, M.R. Kaus, S.J. Haker, W.M. Wells, F.A. Jolesz and R. Kikinis, "Statistical validation of image segmentation quality based on a spatial overlap index1," *Academic Radiology*, vol. 11, no. 2, pp. 178-189, 2004.
DOI: https://doi.org/10.1016/S1076-6332(03)00671-8